ACS APPLIED MATERIALS & INTERFACES

RESEARCH ARTICLE

www.acsami.org

Methylene Green Electrodeposited on SWNTs-Based "Bucky" Papers for NADH and L-Malate Oxidation

Claudia W. Narváez Villarrubia,[†] Rosalba A. Rincón,[†] Vinod K. Radhakrishnan,[‡] Virginia Davis,[‡] and Plamen Atanassov*[,†]

[†]Department of Chemical and Nuclear Engineering, University of New Mexico, Albuquerque, New Mexico 87106, United States

[‡]Department of Chemical Engineering, Auburn University, Auburn, Alabama 36849, United States

ABSTRACT: This research introduces a cavity anode design based on new single-walled nanotube (SWNTs) papers, "bucky" papers, used for the oxidation (and regeneration) of nicotinamide adenine dinucleotide (NADH) and the oxidation of L-malate. The materials designed are paper-like processed composites containing also additives: BP11 sample contains SWNTs and isopropanol (IPA); the BPMG sample contains SWNTs, IPA, and methylene green (MG). NADH/NAD$^+$ is the cofactor responsible for the oxidation of L-malate by malate dehydrogenase (MDH), in the Krebs' cycle. Because of the high overpotential of NADH oxidation, poly methylene green (PMG) was utilized as the electrocatalyst to produce NAD$^+$. The electrocatalyst was deposited on the surface of the "bucky" papers by electropolymerization by means of 10 voltammetric cycles in a range of −0.5 V and +1.3 V (vs Ag/AgCl reference electrode) at a scan rate of 5 mV/s. The catalytic performance of PMG was evaluated by chronoamperometric measurements of NADH oxidation at 0.3 V in phosphate buffer and L-malate oxidation at 0.1 V in the presence of MDH. For both "bucky" papers, the chronoamperometric curves of PMG, current vs NADH concentration, show a linear relationship demonstrating to have a first order Fick's law behavior for concentrations of NADH lower than 6 mM. The chronoamperometric curves in the presence of MDH, current against L-malate concentration, show a Michaelis−Menten behavior where no inhibition or competitive reaction are detected. Additionally, the anodic materials were characterized by scanning electron microscopy (SEM) and energy-dispersive X-ray spectroscopy (EDS), the polymerization of MG is effectively observed in the form of particles nucleation. The anodes show an excellent electrocatalytic activity toward NADH oxidation. The electrode design is feasible, reproducible, and overall stable.

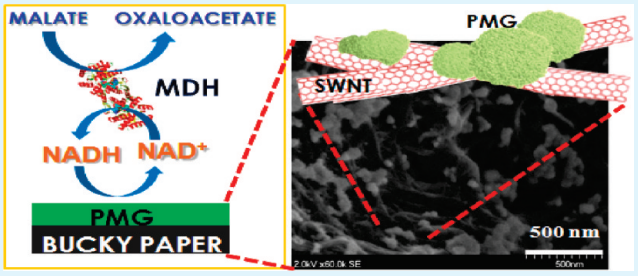

KEYWORDS: carbon nanotube, bucky paper, electrochemical deposition, chronoamperometry, Krebs' cycle, NADH, L-malate dehydrogenase, poly(methylene green), Fick's law, Michaelis−Menten kinetics

INTRODUCTION

Enzymatic-biofuel cells make use of enzymes as catalysts for anodic or cathodic electrochemical processes that work with natural biofuels such as sugars and alcohols.[1] This research introduces the use of single-walled carbon nanotube (SWNTs)-based materials named "Bucky Papers" and the design of an anodic electrode to achieve the oxidation of nicotinamide adenine dinucleotide (NADH) cofactor and L-malate oxidation catalyzed by malate dehydrogenase (MDH) to mimic one of the steps of the Krebs' cycle, which is one of nature's pathways for enzymatic breakdown of complex biofuels like sugars or alcohols.

Carbon nanotubes are promising electrode materials for biofuel cells because of the combination of their high electrical conductivity, mechanical strength and thermal and chemical stability.[2−9] In addition, their small diameters result in both high surface to volume ratios and favorable interactions with similarly sized enzymes. Recent investigations have demonstrated both immobilization of enzymes on carbon nanotubes and direct electron transfer (DET).[1,4,5] These promising initial results provide an impetus for engineering hierarchically ordered carbon nanotube structures with controlled surface chemistry.[2,3,10] Optimum carbon nanotube electrodes must simultaneously satisfy several competing criteria: high electrical conductivity, significant attractive interactions with enzymes, high surface to volume ratio, and sufficiently large pore size to facilitate mass transport. Engineering a system that meets these criteria requires fundamental understanding of the combined effects of nanomaterial chemical structure, dispersion state, processing path, and processing conditions on carbon nanotube electrode structure and enzyme/carbon nanotube interactions.

In this work, a combination of SWNTs and isopropanol (IPA) and methylene green (MG) was used to create an electrode design consisting of hierarchically ordered carbon nanomaterials with controlled surface chemistries. The SWNTs provide high electrical conductivity and enzyme interaction,[7] whereas the other materials facilitate formation of a range of pore sizes; the larger pore sizes facilitate mass transport.

Received: March 12, 2011
Accepted: June 13, 2011
Published: June 13, 2011

dx.doi.org/10.1021/am2003137 | *ACS Appl. Mater. Interfaces* 2011, 3, 2402–2409

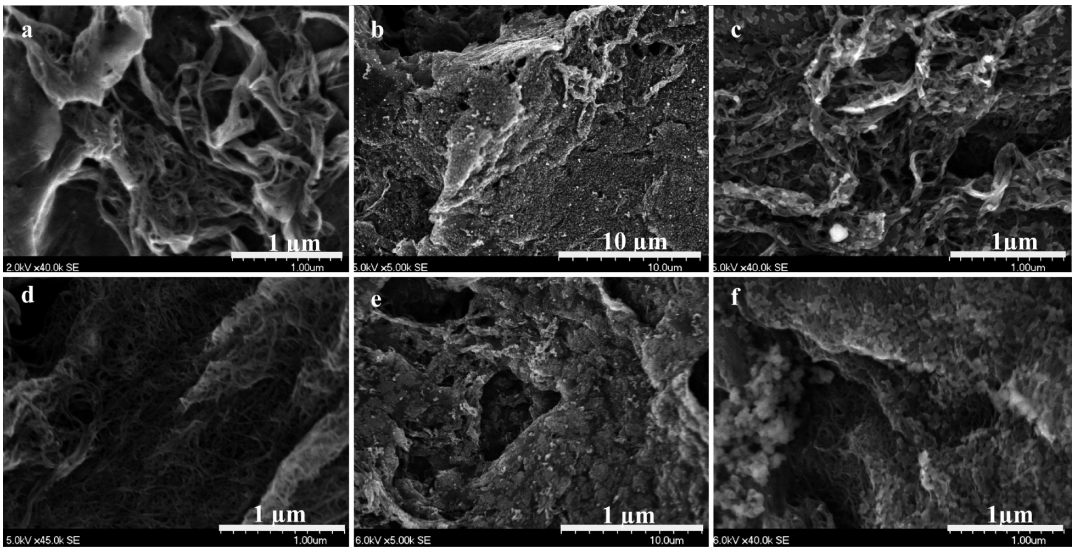

Figure 1. SEM Images of (a) BP11 (SWNTs + IPA) and (d) BPMG (SWNTs + IPA + MG) of surface electrodes before MG electrodeposition and (b, c) BP11-MG and (e, f) BPMG-MG of surface electrodes after MG electrodeposition.

By mimicking the Krebs' cycle, an enzymatic-biofuel cell will produce electric energy using low-cost organic natural sources.[1,11−13] In nature, the Krebs' cycle is a pathway in which a cascade of redox reactions catalyzed by enzymes produces a flux of electrons in the oxidation of organic compounds such as sugars and alcohols. Most enzymes in the Krebs' cycle are NAD^+ -dependent enzymes. In this research, malate dehydrogenase (MDH) is used to oxidize L-malate (substrate) to Oxaloacetate. The L-malate oxidation is a reaction coupled to the reduction of NAD^+ to NADH, where NAD^+/NADH acts as a cofactor. Thus, the performance of MDH is conditioned to the availability of NAD^+. However, the oxidation of NADH to NAD^+ has been a major challenge to overcome during the past decades because of the slow kinetics of the reaction occurring at large overpotentials and the corrosion of the bare electrode oxidation.[14−23] As consequence, it is imperative to design a sensitive and stable electrode that promotes a low overpotential using a mediator[24−39] that catalyzes the oxidation of NADH to NAD^+ (and its regeneration) and prevents the corrosion of the electrode material.

Previous studies have demonstrated that CNTs lowered the potential of NADH oxidation detection[52] and showed to behave similarly to edge plane pyrolytic graphite electrodes.[53] Further studies with NADH catalyst were performed showing the successful NADH oxidation by poly(1,2-diaminobenzene) (1,2-DAB) modified glassy carbon electrodes[53] and 1,2-DAB electropolymerized on CNTs;[54] those results reported to lower the NADH oxidation detection. The functionalization of carbon nanotubes with thionine molecules,[56] a phenotiazine dye, by $\pi-\pi$ stacking interactions between thionine and carbon nanotube conjugated structure[55] showed to decrease the NADH oxidation potential as well. Later, studies of basal plane pyrolytic graphite and CNTs electrodes with adsorbed toluidine blue and azure C, also phenothiazine dyes, were reported for the detection of NADH oxidation showing that the CNTs-based electrodes have better performance toward NADH detection, lower potential and higher currents of NADH oxidation.[57]

To overcome the obstacles presented by the kinetics of the NADH oxidation[15−17] and the MDH performance, this research focused on the design of a stable anodic electrode based on SWNT papers and a mediator. The electrocatalyst employed was poly methylene green (PMG), a highly stable electroactive phenotiazine with catalytic activity for this redox reaction.[24,40−43] During the past few years, substantial effort was placed in investigating the structure and catalytic activity of such PMG catalytic materials.[43−46] The PMG was deposited on the surface of the "bucky" papers[47−49] by electrochemical polymerization of the methylene green (MG) monomer.[50] The performance of the electrode toward NADH oxidation and L-Malate oxidation was tested by applying chronoamperometric measurements.[51] An additional characterization of the materials was developed by scanning electron microscopy (SEM) and energy-dispersivee X-ray spectroscopy (EDS) for further understanding of the "bucky" paper-MG electrode.

EXPERIMENTAL METHODS

Apparatus. The electrochemical experiments were performed in a three-electrode cell by conventional potentiostats: Gamry Reference 600 Pontentiostat/Galvanostat/ZRA and Princeton Applied Research VersaSTAT 3 potentiostat/galvanostat. All potentials are reported vs Ag/AgCl. The material characterization was performed using a scanning electronic microscope Hitachi (S-5200) equipped with an energy dispersive spectrometer (EDS).

Chemicals. HiPco SWNTs were obtained from Unidym Inc. (Menlo Park, CA) and had a length to diameter (aspect) ratio of ∼600 and a purity of ∼90%. Isopropanol (purity >99%), Methylene Green (MG) Zinc Chloride double salt (purity >99%, from Fluka Cat. 66870), NADH (purity ∼98%, Sigma Cat. N6005), NAD+ (purity ∼98%, Fluka Cat. 43407), Lyophilized Malate Dehydrogenase (MDH) from porcine heart (activity 2700un/mg protein, USB products from Affymetrix Cat. 18665) and L-(−)-malic acid (Sigma Cat. M1000) were used without further purification. KNO_3, $NaNO_3$, and monobasic and dibasic sodium phosphates were obtained from EMD Chemicals Inc. and used to prepare the pH 7 phosphate buffer stock solution. TRIS buffer at pH 7 was made from tris(hydroxymethyl)aminomethane (EMD Chemicals 9210) and hydrochloric acid 1.0 N (VWR 7647−01−0) and was used to prepare the MDH enzyme stock solution. L-Malic acid was prepared with distilled water and its pH was adjusted to 7.1 with concentrated NaOH solution.

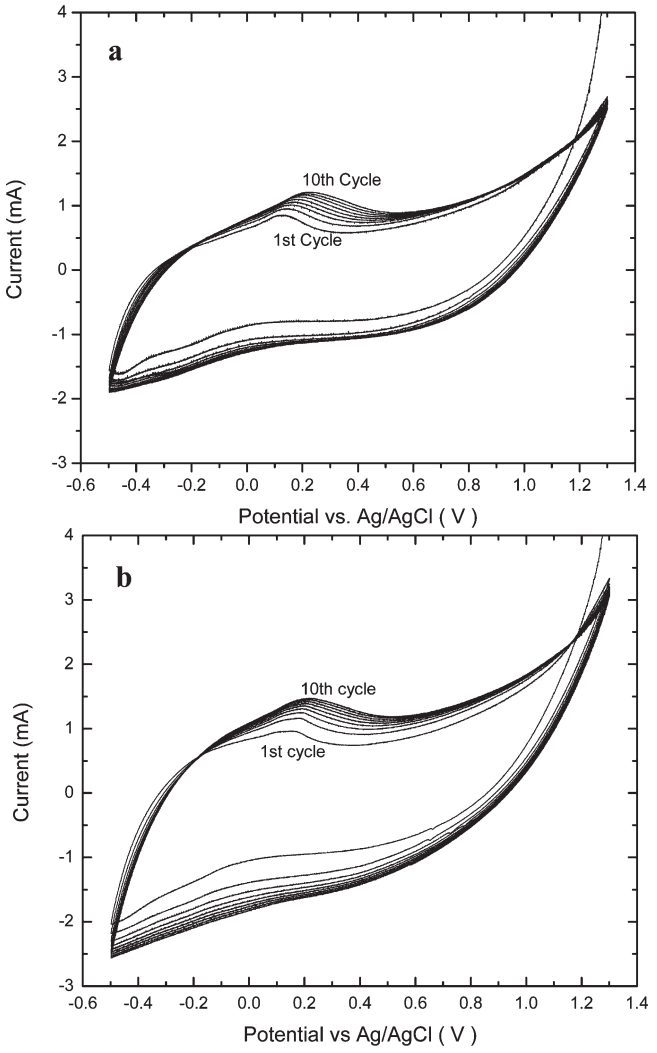

Figure 2. Electrodeposition of MG at 5 mV/s between −0.35 to 1.3 V on (9a) BP11 (SWCNTs+IPA), (b) BPMG (SWCNTs+IPA+MG). The peak shift indicates the polyrization reaction takes place.

CNT Papers—"Bucky" Papers. Two types of SWNT "bucky" papers[47,48] were fabricated for and employed in this work. BP11 "bucky" paper was fabricated by magnetically stirring 60 mg of purified HiPCo SWNTs in isopropanol (1 mg/mL) for three days to produce a uniform dispersion of small bundles. Then, the dispersion was filtered through a 0.2 μm PTFE filter paper. The BPMG "bucky" paper was fabricated by stirring 60 mg of SWNTs and 13 mg of MG in isopropanol (1 mg/mL) followed by filtering the suspension through a 0.2 μm PTFE filter paper. The "bucky" papers were dried at room temperature for 15 min, peeled off the filter paper, and vacuum-dried overnight at 80 °C. The thickness of the "bucky" papers was measured to be approximately 350 μm.

To maintain the SWNTs' pristine properties, no sonication or functionalization was performed. The SWNTs were stirred in isopropanol to break up large nanotube aggregates while still retaining large ropes of nanotubes. The presence of nanotube ropes in the "bucky" paper increase the porosity of the "bucky" paper, thus facilitating enhanced transport of materials while still preserving a network for electrical conductivity. The MG and SWNTs were stirred together, prior to filtration, in order to distribute MG evenly though the nanotubes and to maximize interfacial contact between the SWNTs and MG.

Electrode Design. The cavity electrode design was chosen for this study. 50% teflonized carbon powder (XC50) was used as adherent material and compacted into the cavity of the electrode. Then, a piece of "bucky" paper that fitted the cavity diameter was placed and pressed on top of the compacted XC50 and adhered to it. The "bucky" paper's surface was further modified by PMG deposition.

The PMG was deposited on the surface of the "bucky" papers by electrochemical deposition in a three electrodes cell, where Ag/AgCl (CH Instruments Inc. Cat. CHI111) and Pt (0.127 mm and purity 99.9% Alfa-Aesar Cat. 10282) were the reference and counter electrodes used respectively and the "bucky" paper cavity electrode played as the working electrode. The electrodeposition was performed by means of 10 cyclic voltammograms[36] at a scan rate of 5 mV/s within −0.5 to 1.3 V range following the standard protocol by Svoboda et al.[49] The MG growing solution consisted of 0.5 mM MG and 0.1 M KNO_3 dissolved in 10 mL of 50 mM sodium phosphate buffer solution at pH 7. The process was performed in absence of oxygen to avoid the oxidation of the polymer; nitrogen was used to deplete oxygen from the growing solution. Similar steps were used with rotating disk electrode (RDE) at 1600 rpm. By following this procedure, the BP11-MG and BPMG-MG electrodes were created.

Hydrodynamic Polarization Curves. In order to find the working potential at which PMG on the electrodes oxidizes NADH and MDH oxidizes L-Malate, hydrodynamic polarization curves were developed using both BP1l-MG and BPMG-MG electrodes for the static as well as the RDE at 1600 rpm. The curves were obtained by plotting the measured current against the respective potential. The steady state currents were measured by applying constant potentials that ranged from −0.05 to 0.35 V by increments of 0.05 V. For NADH, the current was measured in 10 mL cells of 1 mM NADH, 10 mM NADH and a blank of phosphate buffer for both electrode materials, BP11-MG and BPMG-MG.

Cyclic Voltammetry for NADH oxidation. With 10 mM NADH in solution in a 10 mL cell, cyclic voltammetric curves (CVs) were taken at a scan rate of 20 mV/s between −0.5 V and 0.5 V of potential range for the electrode BP11-MG (shown) and BPMG-MG (not shown). To evaluate the performance of the electrodes, the first blank was performed in phosphate buffer for the electrodes with MG polymerized on the surface. The second blank was performed in 10 mM NADH in solution for the electrode without MG polymerized on the surface.

Chronoamperometry for NADH Oxidation. The concentration of the NADH stock solution was determined and used in chronoamperometric measurements. The concentration of the NADH stock solution was found by measuring the absorbance of this compound applying UV−vis spectroscopy and the law of Lambert−Beer. This law establishes a linear relationship ($A = \varepsilon bC$) between the UV−vis absorbance of a compound to its concentration, C (molar units, M), its molar absorptivity, ε ($M^{-1}cm^{-1}$) and the width of the cuvette, which contains the sample (cm). The concentration was determined at the highest absorbance peak, close to unity, in the UV−vis spectrum in a 300−500 nm wavelength (λ) range. The absorbance peak for NADH was found at λ = 340 nm. Its concentration was easily found since the absorptivity for NADH is $\varepsilon = 6300\ M^{-1}\ cm^{-1}$ at standard condition and the conventional cuvette has 1 cm of width. The absorbance measured was effectively linearly dependent on the concentration in the 0 to 6 mM NADH range; high concentrations of NADH showed high absorbance. The performance of the electrodes was then analyzed by chronoamperometry.

Chronoamperometric curves were obtained by monitoring the current generated by consecutive periodic addition of NADH or L-Malate aliquots to the electrolytic cell as a function of time. 0.3 V, ideal working potential found through the hydrodymamic polarization curves, was applied to evaluate the performance of the electrodes for the NADH oxidation. This experiment consisted of adding aliquots of 58 mM NADH solution (NADH stock solution) to the electrochemical cell which initially contained 10 mL of phosphate buffer solution. Before the first aliquot of NADH was added to the cell and after each posterior addition, the system showed steady -state current behavior. Each

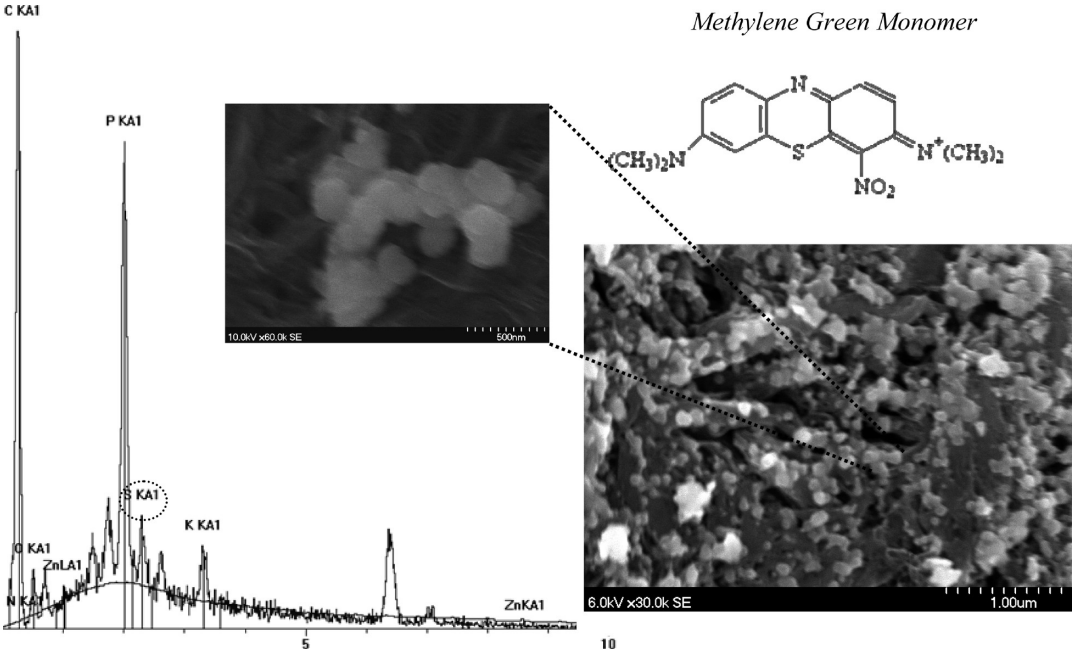

Figure 3. EDS spectrum of the surface of BP11-MG Electrode.

addition was made in a time interval of 500 s to allow the system to approach steady state. The currents were measured after each aliquot added and were plotted against the respective concentration of the NADH in the cell.

Chronoamperometry for L-Malate Oxidation. Chronoamperometric measurements were also developed to evaluate the MDH behavior using the BP11-MG and BPMG-MG electrodes. For the evaluation of the enzyme performance in solution, the current was monitored for each aliquot of the L-Malate (substrate) added to the electrolytic cell where a constant 0.1 V voltage was applied. Initially, the cell contained 50 μL of enzyme dissolved in TRIS buffer in a proportion of 1 mg:100 μL respectively, 10 mL of 10 mM NAD^+ dissolved in phosphate buffer at pH 7 and 45.0 $\pm$ 0.1 mg KNO_3. In this step, each aliquot of 1 M L-Malate was added to the cell after the steady state current was approached in time intervals of 400 s. The measured steady state current was plotted as a function of the respective substrate concentration. The mentioned procedure is used to gather data to evaluate the kinetic behavior of the MDH enzyme in solution in the oxidation of L-Malate using the "bucky" papers electrodes BP11-MG and BPMG-MG.

RESULTS AND DISCUSSION

Resistivity, Wettability, and SEM Imaging of "Bucky" Papers. BP11 showed a resistivity of 14.7 mΩ/ mg and BPMG 47.2 mΩ/ mg; a copper (Cu) wire was used as a blank. As expected, both "bucky" papers show low resistivity demonstrating their high quality as conductor material for the design of our electrodes.

The SEM micrographs show how the strains of SWNTs effectively conferred a high surface area to the "bucky" papers and high porosity due to the bundles formed by the nanotubes (images a and d in Figure 1). There were no treatment or conductive coatings performed on the samples prior to SEM observations. The combination of porosity provided by the SWNTs and hydrophilicity provided by the IPA conferred high wettability to the "bucky" papers. BP11 and BPMG were easily wetted but BPMG showed to be more hydrophilic than BP11 due to the presence of MG (highly hydrophilic and soluble in water).

Table 1. EDS Data of the Surface of BP11-MG Electrode, Composition of the Elements Deposited on the Carbon SWNT Electrode

	O	K	P	S	Zn	total
wt %	36.84	10.53	42.11	5.26	5.26	100

Because of their porosity and their hydrophilicity, both materials are fragile. Despite their fragility, they were easily used in the fabrication of these cavity anodes.

Methylene Green Electrodeposition. MG was deposited on the surface of the "bucky" papers by means of 10 voltammetric cycles within −0.5 and 1.3 V at 5 mV/s of scan rate. The oxidative peak of MG is observed at 0.12 V in the first cycle and 0.2 V in the 10th cycle on both BP11 and BPMG papers for the static (not shown) as well as the RDE (Figure 2) electrodes. The displacement of the oxidative peak indicates that an oxidative polymerization is taking place and more electroactive species are being deposited on the surface of the electrode.[5,43] A background was also performed in this step using XC50-Carbon Black and XC50 (not shown). On both "bucky" papers, the MG electrochemical deposition generates a nucleation of PMG that results in the formation of particles observed on their surface by SEM imaging (images b and c for BP11-MG and e and f for BPMG-MG in Figure 1).

When compared to previous studies, the electrodeposition of the mediator (MG) shows to have a higher charge transferred for the reaction. For the deposition of the mediator monomer, previous studies have shown CVs with oxidation peaks of MG deposition at ~ -0.05 V/cm^2 with a current of $\sim$720 μA/cm^2 for the first cycle and a potential of $\sim$0.22 V/cm^2, with a current density of $\sim$325 μA/cm^2 for the last cycle on glassy carbon electrodes (vs Ag/AgCl).[46] In this research the electro-polymerization peaks have been registered at +0.12 V and a current of 0.95 mA ($\sim$ 2.47 mA/cm^2 for a geometric electrode radius of 3.5 mm) is observed; the curve moves toward more positive potentials as the number of cycles increase. The last cycle is

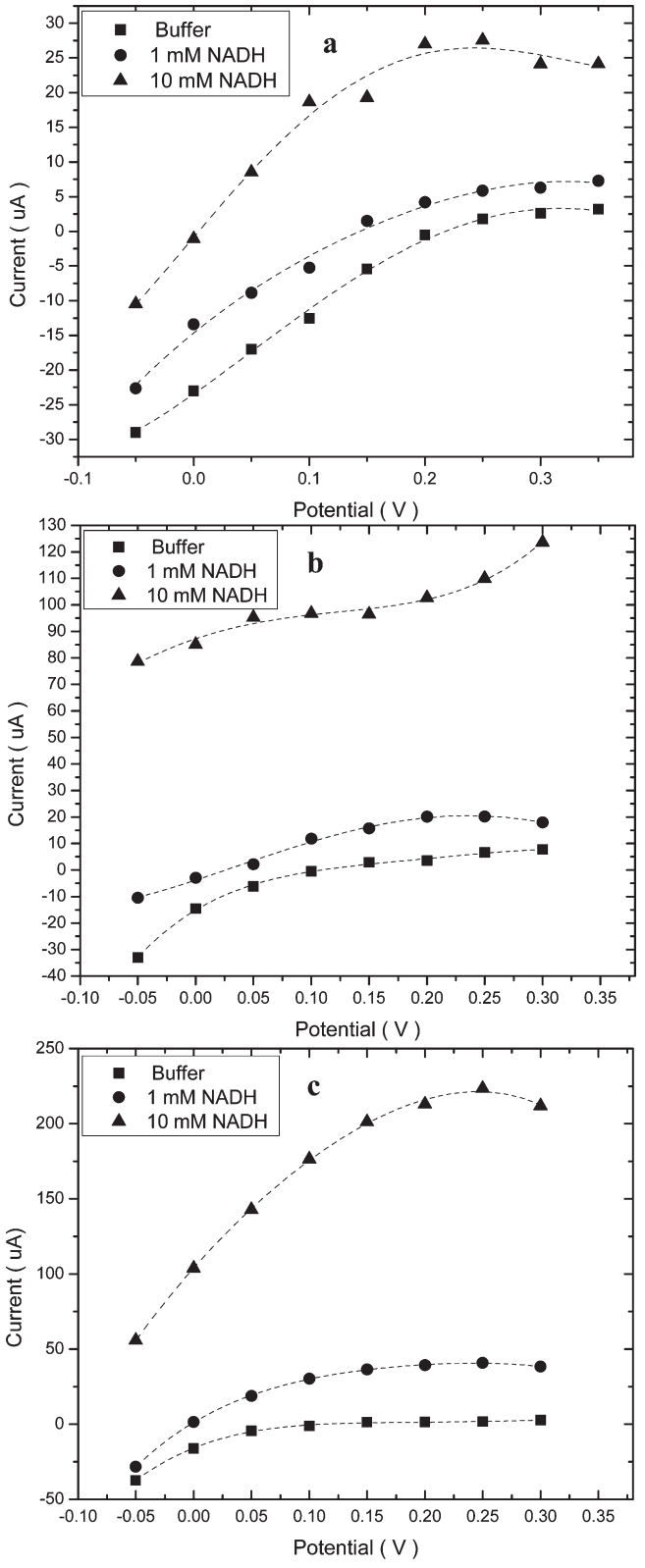

Figure 4. Hydrodynamic polarizationn curves with sodium phosphate buffer, NADH 1 mM, and NADH 10 mM on (a) BP11-MG Electrode, (b) BPMG-MG electrode, and (c) BPMG-MG RD electrode at 1600 rpm.

found at +0.2 V and a current of 1.2 mA (vs Ag/AgCl) is obtained.

The EDS techniques were applied to corroborate the polymerization of MG was successfully performed. By SEM imaging, the particles of polymers are observed on the surface of the material (b and c for BP11-MG and e and f for BPMG-MG in Figure 1) which shows a noticeable difference compared to the initial clean surface-material shown in Figure 1 images a and d for BP11 and BPMG respectively. The particles vary from 10−20 nm to 1 μm (Figure 1c,f) and are uniformly distributed on the "bucky" papers surface. Because electrolytic salts are used in the process of polymerization, it is logic to believe the nucleation observed may be due to the precipitation of electrolytes. Because of this reason, a further analytical study by EDS was performed applying a 10 KeV beam. For this analysis, the structure of the MG monomer was taken into account and from it, Sulfur (S) and Zinc (Zn) were traced on the BP11 surface (Figure 3). In this case, the presence of sulfur and zinc on the surface would demonstrate an effective polymerization because MG is the only source of them. The EDS spectrum demonstrated that MG was successfully deposited on the BP11 (Figure 3); Table 1 shows that sulfur constituted the 5.26% of the total deposited compounds to the BP11 paper surface as well as zinc (5.26%). BPMG is expected to have MG deposited on its surface as well since the same procedures were applied in its process. To corroborate these results and that no other compound was deposited, the "bucky" papers were subjected to cyclic voltammetry in a background solution without the MG monomer. These solutions contained the buffer and KNO_3 in similar quantities than the MG growing solution. After exposing the material to 10 voltammetric cycles, the surface of the BP11 was analyzed through SEM imaging and EDS. SEM images showed that there was precipitation of electrolytes, there were sporadic formations of particles on the BP11 surface (not shown). However, the EDS analysis showed presence of neither sulfur nor zinc (spectrum not shown). The EDS shows that meaningless amounts of electrolytes in the growing solution precipitated on the "bucky" paper's surface but PMG was successfully deposited (Figure 3). Further chroanoamperometric measurements confirmed the MG polymerization on BP11 and BP-MG and show the PMG performance as mediator in the anodic process.

Hydrodynamic Polarization Measurements. By constructing a hydrodynamic polarization curve, the ideal working potential for NADH was determined for both BP11-MG and BPMG-MG electrodes. For the BP11-MG electrode, the working potential found was 0.3 V (Figure 4a); this was applied to perform chronoamperometric measurements for NADH. For a 10 mM NADH the current is proportionally increased with the concentration of NADH compared to 1 mM NADH and the buffer background. In Figure 4b, the compositional material MG proved to induce an increment in the current generated at the same potential range of testing (−0.05 to 0.35 V). The current measured is approximatelly 95 μA at 0.2 V on BPMG-MG electrode (Figure 4b) while the current measured for BP11-MG electrode is approaching 25 μA at 0.3 V (Figure 4a), both experiments performed with 10 mM of NADH. Evenmore, comparing both curves with the BPMG-MG at 1600 rpm (RDE) and mantainning constant all other conditions, the graph shows an increment on the current measured to 225 μA at 0.2 V on BPMG-MG (Figure 4-c), demonstrating the mass transport dependence of the oxidative process with respect to the electrode material design. The increment of the current measured with BPMG-MG demonstrates that the high amount of MG in this material induces a larger number of NADH oxidative reactions per surface area and unit

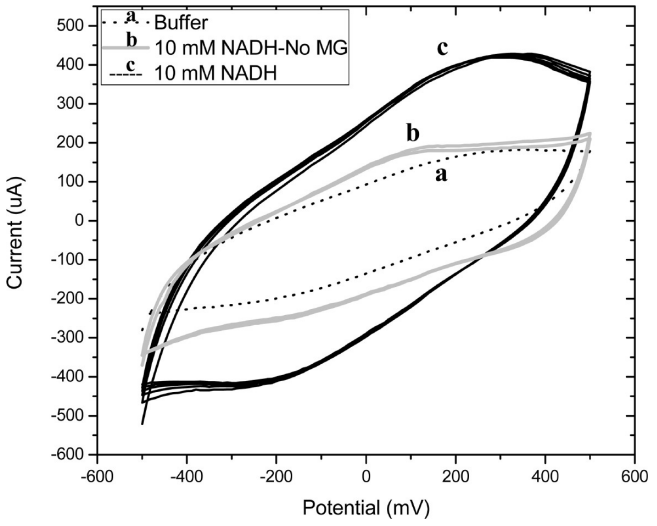

Figure 5. Cyclic voltammetric curves for NADH oxidation: (a) BP11-MG electrode in sodium phosphate buffer, (b) bare BP11 in 10 mM NADH, and (c) BP11-MG in 10 mM NADH.

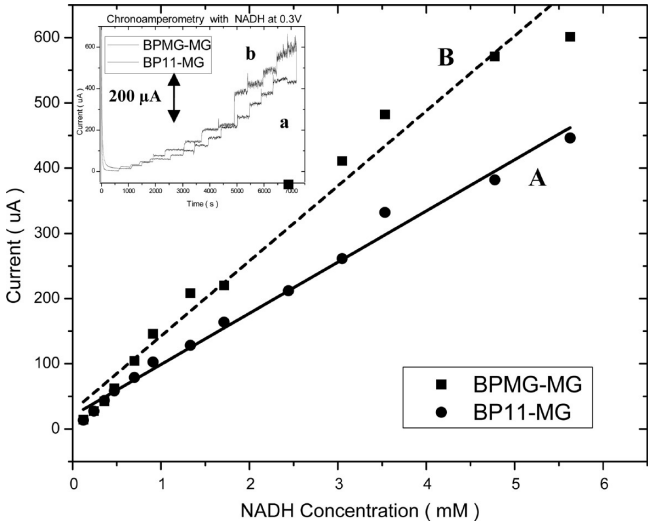

Figure 6. Relationship between Current generated and NADH Concentration (mM) on (A) BP11-MG, (B) BPMG-MG Electrodes found by Chronoamperometry with NADH on (a) BP11-MG and (b) BPMG-MG Electrodes. The first Fick's law behavior is observed.

time, but does not make the material a better condutor when compared to BP11-MG.

Cyclic Voltammetry with NADH. The CVs for NADH shown in Figure shows the NADH can be oxidized at 0.2 V (200 mV) with a current measured of approximately 400 μA for the BP11-MG electrode (curve c, Figure 5). The CV for the BP11 in NADH (second blank) shows a low current measured and lower catalytic activity toward NADH oxidation compare (curve b, Figure 5). The activity showed by this electrode is close to the behavior showed by the BP11-MG in absence of NADH (first blank, curve a in Figure 5). These results demonstrate the catalytic activity of the BP11-MG toward NADH oxidation.

Chronoamperometry with NADH. The chronoamperometric curves (Figure 6) were used to find the relationship of the current

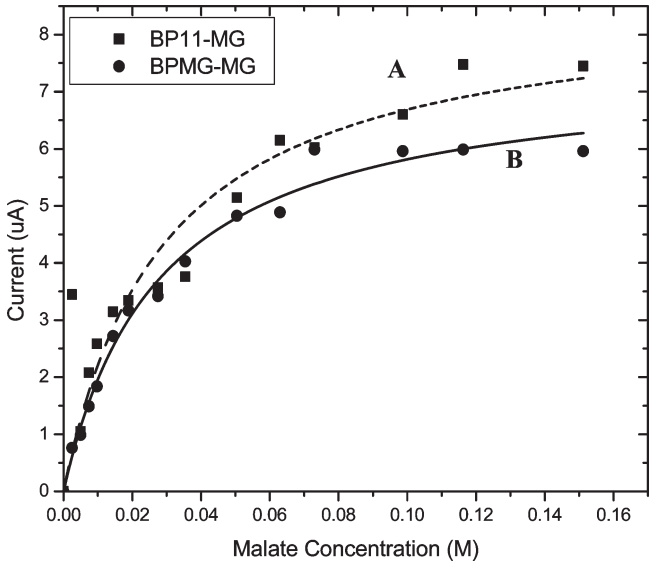

Figure 7. Relationship between current generated and L-malate concentration (M) on (A) BP11-MG (dashed line), (B) BPMG-MG (solid line) electrodes found by chronoamperometry with MDH. Michaelis–Menten kinetics, there are neither inhibitors nor competitive processes.

Table 2. EDS Data of the Surface of BP11-MG Electrode, Composition of the Elements Deposited on the Carbon SWNT Electrode

	I_{max}I(μA)	K_M(M)
BP11-MG	8.6 ± 0.9	0.029 ± 0.009
BPMG-MG	7.4 ± 0.3	0.028 ± 0.003

generated with respect to the concentration of NADH in the cell. The generated currents demonstrate there was a catalytic activity produced by the PMG on the surface of the "bucky" papers (BP11 and BPMG). An increasing stepped current was observed that was due to the catalyzed oxidation of NADH, which produced a shuttle of electrons when each NADH aliquot was added to the cell. The linear relationship shown in Figure 6 demonstrates that the system follows the first order Fick's law within the range of concentration measured (0 to 6 mM NADH).

Chronoamperometry with MDH by Additions of L-Malate. Chronoamperometric measurements were performed to evaluate the enzymatic activity of MDH in solution in the presence of PMG electrocatalyst. After each consecutive addition of aliquots of 1 M L-malate (at steady state), the currents were recorded and plotted against the substrate concentration. Initially, in the cell, MDH and its diffusive cofactor NAD+ were in solution at a concentration of 0.5 mg in 50 μL of MDH and 10 mL of 10 mM NAD+ respectively. The enzyme shows a typical Michaelis–Menten behavior at 0.1 V potential (Figure 7). The Michaelis–Menten constant of MDH was found to be K_M = 0.029 ± 0.009 M using the BP11-MG anode and K_M = 0.028 ± 0.003 M using the BPMG-MG anode (Table 2). The maximum current generated are I_{max} = 8.6 ± 0.9 μA for BP11-MG and I_{max}= 7.4 ± 0.3 μA for BPMG-MG at the given conditions (Table 2). Previous studies have reported a maximum current density of 1.55 μA/cm^2 for a potential of 0.1 V at a concentration of L-malate of 700 mM in the cell for MDH in solution as well.[46] This research presents a maximum current of 8.6 μA for BP11-MG (current density of

22.35 μA/cm^2 for an geometric electrode radius of ~3.5 mm) and 7.4 μA (current density of 19.23 μA/cm^2 for the same electrode radius) obtained for BPMG-MG anodes 160 mM of L-malate concentration (at 0.1 V as well). This is approximately 20-fold improvement with respect to the existing art. It is observed that the performance of the anodes presented here showed successful oxidation of the substrate L-malate by the MDH dehydrogenase. This is possibly due to the availability of the NAD+ (through catalysis by PMG) in solution and to the improved enzyme/substrate/electrode surface interaction. These results were obtained at steady state condition for each measurement and within an interval of 2 h overall showing the NAD+ is recycled in the process and PMG and MDH enzyme are catalytically active within that interval of time. The enzymatic process shows there are neither inhibitors nor competitive processes occurring in the substrate oxidation reaction.

CONCLUSION

The new SWNTs materials, "bucky" papers, were satisfactorily fabricated and effectively applied to the design of a cavity bioanode and could be further used in the development of a biofuel cell. The catalytic activity of PMG was observed during chronoamperometric measurements of oxidation at 0.3 V for NADH and 0.1 V for L-malate oxidation by MDH in solution. The oxidation of the NADH by the catalytic activity of PMG follows the first Fick's Law at low concentrations. The Michaelis−Menten behavior of the enzyme shows no inhibition or competitive processes during the oxidation of the substrate and no processes affecting the electrodes performance. The oxidation and regeneration of NADH cofactor during the oxidation of L-Malate was satisfactorily catalyzed by PMG electrodeposited on the "bucky" papers' surface. By immobilizing the enzyme on the electrode surface, the performance and stability of the enzyme could be improved; highly efficient electrode/active site/substrate interactions can be approached.

An improvement of the fabrication of the anode was achieved. The use of SWNTs in the material increase porosity and the surface area of the material providing an increase in the number of active sites of the catalyst per unit area and improving the mass transfer through the material. The interface interactions at the nanoscale for the reactions happening on the materials surface were improved. The components of the BP11 and BPMG (SWNTs, IPA and SWNTs, IPA and MG, respectively) are well-combined to give a conductive-hydrophilic-porous-manageable material for this cavity anode design. The incorporation of the MG monomer has effectively provided an increase of the number of oxidative NADH reactions, increasing the number of electrons shuttled to the cathode and showing an increase in measured current. The incorporation of the monomer into the material opens the door for improvement and would simplify the manufacturing process of the cavity anode material based in SWNTs. This research increased the understanding of the SWNT materials to enable biofuel cell electrodes with greater reproducibility and efficiency.

AUTHOR INFORMATION

Corresponding Author

*CORRESPONDING AUTHOR FOOTNOTE Plamen Atanassov University of New Mexico Department of Chemical & Nuclear Engineering MSC01 1120; 209 Farris Engineering Center Albuquerque, NM 87131 Phone: (505) 277-2650; Fax: (505) 277-5433 E-mail: plamen@unm.edu.

ACKNOWLEDGMENT

The authors gratefully acknowledge financial support from the AFOSR MURI Program in Fundamentals and Bioengineering of Enzymatic Fuel Cells.

REFERENCES

(1) Minteer, S. D.; Liaw, B. Y.; Cooney, M. J. *Curr. Opin. Biotechnol.* **2007**, *18*, 228.
(2) Dai., H.; Kong, J.; Zhou, C.; Franklin, N.; Tombler, T.; Cassel, A.; Fan, S.; Chapline, M. *J. Phys. Chem.* **1999**, *103*, 11246.
(3) Dai, H. *Acc. Chem. Res.* **2002**, *35*, 1035.
(4) Guiseppi-Elie, A.; Lei, C.; Ray, B. H. *Nanotechnology* **2002**, *13*, 559.
(5) Ivnitski, D.; Branch, B.; Atanassov, P.; Apblett, C. *Electrochem. Commun.* **2006**, *8*, 1204.
(6) Yan, Y.; Zheng, W.; Su, L.; Mao, L. *Adv. Mater.* **2006**, *18*, 2639.
(7) Yan, J.; Zhou, H.; Yu, P.; Su, L.; Mao, L. *Adv. Mater.* **2008**, *20*, 2899.
(8) Li, X.; Zhou, H.; Yu, P.; Su, L.; Ohsaka, T.; Maoa, L. *Electrochem. Commun.* **2008**, *10*, 851.
(9) Vichchulada, P.; Zhang, Q.; Duncan, A.; Lay, M. D. *ACS Appl. Mater. Interfaces* **2010**, *2*, 467.
(10) Zhao, Z.; Gou, J.; Khan, A. *J. Nanosci.* **2009**, No. 325769.
(11) Atanassov, P.; Apblett, C.; Banta, S.; Brozik, S.; Barton, S. C.; Cooney, M. J.; Liaw, B. Y.; Mukerjee, S.; Minteer, S. D. *Electrochem. Soc. Interfaces* **2007**, *16*, 28.
(12) Sokic-Lazic, D.; Minteer, S. D. *Biosens. Bioelectron.* **2008**, *24*, 939.
(13) Sokic-Lazic, D.; Minteer, S. D. *Electrochem. Solid-State Lett.* **2009**, *12*, F26.
(14) Blaedel, W. J.; Haas, R. G. *Anal. Chem.* **1970**, *42*, 918.
(15) Leduc, P.; Thévenot, D. *Bioelectrochem. Bioenerg.* **1974**, *1*, 96.
(16) Blaedel, W. J.; Jenkins, R. A. *Anal. Chem.* **1975**, *47*, 1337.
(17) Moiroux, J.; Elving, P. J. *J. Am. Chem. Soc.* **1980**, *102*, 6533.
(18) Jaegfeldt, H. *J. Electroanal. Chem.* **1980**, *110*, 295.
(19) Elving, P. J.; Bresnahan, W. T.; Moiroux, J.; Samec, Z. *Bioelectrochem. Bioenergy* **1982**, *9*, 365.
(20) Blankespoor, R. L.; Miller, L. L. *J. Electroanal. Chem.* **1984**, *171*, 231.
(21) Gorton, L.; Hale, P. D.; Persson, B.; Boguslavsky, L. I.; Karan, H. I.; Lee, H. S.; Skotheim, T. A.; Lan, H. L.; Okamoto, Y. *ACS Symp. Ser.* **1992**, *487*, 56.
(22) Chenault, H. K.; Whitesides, G. M. *Appl. Biochem. Biotechnol.* **1987**, *14*, 147.
(23) Karyakin, A. A.; Ivanova, Y. N.; Revunova, K. V.; Karyakina, E. E. *Anal. Chem.* **2004**, *76*, 2004.
(24) Gorton, L.; Bartlett, P. N., NAD(P)-Based Biosensors. *Bioelectrochemistry: Fundamentals, Experimental Techniques, And Applications*; Bartlett, P. N., Ed.; John Wiley & Sons: West Sussex, U.K., 2008; pp 157−198.
(25) Gorton, L. *J. Chem. Soc., Faraday Trans. 1* **1986**, *82*, 1245.
(26) Gorton, L.; Csöregi, E.; Domínguez, E.; Emnéus, J.; Jönsson-Pettersson, G.; Marko-Varga, G.; Persson, B. *Anal. Chim. Acta* **1991**, *250*, 203.
(27) Bartlett, P. N.; Tebbutt, P.; Whitaker, R. G. *Prog. React. Kinet.* **1991**, *16*, 55.
(28) Schuhmann, W.; Schmidt, H. L., Amperometric biosensors for substrates of oxidases and dehydrogenases. *Advances in Biosensors*; Turner, A. P. F., Renneberg, R., Eds.; JAI Press: London, 1992; Vol. 1, pp 79−130.
(29) Schuhmann, W.; Huber, J.; Wohlschläger, H.; Strehlitz, B.; Gründig, B. *J. Biotechnol.* **1993**, *27*, 129.
(30) Katakis, I.; Domínguez, E. *Microchim. Acta* **1997**, *126*, 11.
(31) Lobo, M. J.; Miranda, A. J.; Tuñón, P. *Electroanal.* **1997**, *9*, 191.
(32) Lorenzo, E.; Pariente, F.; Hernàndez, L.; Tobalina, F.; Darder, M.; Wu, Q.; Maskus, M.; Abruña, H. D. *Biosens. Bioelectron.* **1998**, *13*, 319.

(33) Armstrong, F. A.; Wilson, G. S. *Electrochim. Acta* **2000**, *45*, 2623.
(34) Habermuller, L.; Mosbach, M.; Schuhmann, W. *Fresenius J. Anal. Chem.* **2000**, *366*, 560.
(35) Gorton, L.; Domínguez, E. *Rev. Mol. Biotechnol.* **2002**, *82*, 371.
(36) Gorton, L.; Domínguez, E. Electrochemistry of NAD(P)+/NAD(P)H. In *Bioelectrochemistry*; Bard, A. J., Stratmann, M., Wilson, G. S., Eds.; Wiley-VCH: Weinheim, Germany, 2002; Vol. 9, pp 67−143.
(37) Palmore, G. T. R.; Bertschy, H.; Bergens, S. H.; Whitesides, G. M. *J. Electroanal. Chem.* **1998**, *443* (1), 155.
(38) Dai, Z. H.; Liu, F. X.; Lu, G. F.; Bao, J. C. *J. Solid State Electrochem.* **2008**, *12* (2), 175.
(39) Prieto-Simon, B.; Fabregas, E. *Biosens. Bioelectron.* **2004**, *19* (10), 1131.
(40) Zhou, D.; Fang, H.-Q.; Chen, H-Y; Ju, H.-X.; Wang, Y. *Anal. Chim. Acta* **1996**, *329*, 41.
(41) Karyakin, A. A.; Karyakina, E. E.; Schuhmann, W.; Schmidt, H. L. *Electroanal.* **1999**, *11* (8), 553.
(42) Karyakin, A.; Karyakina, E. E.; Schmidt, H. L. *Electroanalysis* **1999**, *11*, 149.
(43) Svoboda, V.; Cooney, M. J.; Rippolz, C.; Liaw, B. Y. *J. Electrochem. Soc.* **2007**, *154* (3), D113.
(44) Akkermans, R. P.; Roberts, S. L.; Marken, F.; Coles, B. A.; Wilkins, S. J.; Cooper, J. A.; Woodhouse, K. E.; Compton, R. G. *J. Phys. Chem. B* **1999**, *103* (45), 9987.
(45) Arechederra, M. N.; Jenkins, C.; Rincón, R. A.; Artyushkova, K.; Atanassov, P.; Minteer, S. D. *Electrochim. Acta* **2010**, *55*, 6659.
(46) Rincón, R. A.; Artyushkova, K; Mojica, M.; Germain, M. N.; Minteer, S. D.; Atanassov, P. *Electroanalysis* **2010**, *22*, 799.
(47) Gou, J.; Liang, Z.; Wang, B. *Int. J. Nanosci.* **2004**, *3*, 293.
(48) Gou, J. *Polym. Int.* **2006**, *55*, 1283.
(49) Svoboda, V.; Cooney, M.; Liaw, B. Y.; Minteer, S.; Piles, E.; Lehnert, D.; Barton, S. C.; Rincon, R.; Atanassov, P. *Electroanalysis* **2008**, *20* (10), 1099.
(50) Penner, R. M. *J. Phys. Chem. B* **2002**, *106* (13), 3339.
(51) Moehlenbrock, M. J.; Arechederra, R. L.; Sjöholm, K. H.; Minteer, S. D. *Anal. Chem.* **2009**, *81*, 9538.
(52) Musameh, M.; Wang, J.; Merkoci, A.; Lin, Y. *Electrochem. Commun.* **2002**, *4*, 743.
(53) Banks, C. E.; Compton, R. G. *Analyst* **2005**, *130*, 1232.
(54) Chen, J.; Bao, J.; Cai, C.; Lu, T. *Anal. Chim. Acta* **2004**, *516*, 29.
(55) Badea, M.; Curulli, A.; Palleschi, G. *Biosens. Bioelectron.* **2003**, *18*, 689.
(56) Li, Q.; Zhang, J.; Yan, H.; He, M.; Liu, Z. *Carbon* **2004**, *42*, 287.
(57) Lawrence, N. S.; Wang, J. *Electrochem. Commun.* **2006**, *8*, 71.